NanoAnalysis
An International Journal
Available online at: www.jnanoanalysis.net or www.jnanoanalysis.com

Hydrogen rich gas production via nano-catalytic gasification of bagasse in supercritical water

Ahmad Tavassoli[a*], Masoumeh Ghalbi Ahangari[b]

a- School of Chemistry, College of Science, University of Tehran, Tehran, Iran

b- Research Institute of petroleum Industry, National Iranian Oil Company, Tehran, Iran

Abstract

Ru/Al_2O_3 nano-catalysts were prepared with impregnation and microemulsion techniques. The supercritical water gasification reaction was performed at 400°C and 5-60 min. Within the tested operation conditions, the reaction residence time of 15 min was the optimum to maximize the H_2 yield. It was observed that using microemulsion technique increases the total gas yield significantly. Using microemulsion technique for preparation of Ru/Al_2O_3 nano-catalyst with water to surfactant ration of 0.5, increased the hydrogen yield to 17.6 (mmol of H_2/ g of bagasse), CO yield to 14.2 (mmol of CO/g of bagasse) and light gaseous hydrocarbons to 1.4 (mmol of light gaseous hydrocarbons/g of bagasse). It was observed that using micro emulsion technique increases the catalyst specific activity by a factor of 1.7 which considerably can enhance the economic aspects of the bagasse super critical water gasification technology.

Keywords: Hydrogen, Bagasse, Supercritical water gasification, Ruthenium, Yield

1.Introduction

Due to the increasing price and undesirable environmental effects of fossil fuels, production of energy from renewable resources has gained much attention in recent years. Biomass is considered to be one of the most promising resources for the production of future fuels. In many cases, because of large water content and high drying cost, biomass is not a suitable feedstock for conventional thermo-chemical gasification technologies. Supercritical and hydrothermal gasification processes offer attractive alternatives for the conversion of wet biomass to useful products. During these processes, biomass is hydrolyzed by water into smaller molecules. Therefore, contrary to conventional thermo-chemical processes, drying of biomass is not necessary. Consequently, hydrothermal gasification of a feedstock with as much as 90% water could become an economically favourable process. Furthermore, with the aid of this technology, hydrogen or methane can be generated at an elevated pressure, hence diminishing the need for pressurizing the final gas product [1].
Most commonly used biomass is of plant origin. Real plant biomass is a complex material that typically

* Corresponding Author: Email: tavassolia@khayam.ut.ac.ir, Phone: (98)-21-61113643, Fax: (98)-21-66495291

consists of cellulose, hemicelluloses and lignin. Therefore, various researchers have utilized model compounds; such as cellulose, glucose, xylan, glycerol, p-cresol, and phenol to study the supercritical and hydrothermal gasification processes and a large number of experimental investigations on these model compounds gasification in SCW were conducted [2-7]. They concluded that carbohydrates (i.e. cellulose and hemicelluloses) gasifies much easier than xylen and lignin, and lignin is the most difficult to gasify. [2-7]. Also, it was realized that lignin can interact with cellulose and change both the gas yield and product gas composition [8]. Other researchers expressed that, in SCW gasification of real biomass feedstock, char/coke may originate from not decomposed biomass by a solid–solid conversion and coke formation in biomass gasification process due to the presence of lignin, not only depends on the lignin amount but also strongly depends on the structure of lignin and interactions between other components in the real biomass [9].

These findings clearly reveal that, due to complexity of biomass (real plant biomass typically consists of 25% lignin and 75% cellulose and hemicelluloses), these model compounds are not able to accurately simulate the behavior of real biomass.

Annually, more than six hundred thousand tons of bagasse is burned in Haft Tappe Industries Company in Iran, which creates serious environmental problems and wastes huge amount of energy. There are several methods of utilizing this valuable biomass to generate energy and fuels, however, gasification processes, technologically offer more attractive option for large scale applications and is a more friendly way for using biomass for energy purposes, given that due to the presence of non-oxidation conditions, the pollutant emissions are greatly low[10-23]. Theoretical calculations show that about 64.5 grams of hydrogen can be produced from one kilogram of bagasse. The hydrogen-rich gas produced from bagasse gasification in addition to being an alternative energy source, can be used in Oil, Gas and Petrochemical industries.

Different catalysts have been used for conversion of bio-oil and biomass to fuel gases [24-27]. It was found that ruthenium and nickel catalysts typically used for reforming, had a substantial activity for the conversion of organic matters to fuel gases [24-27]. Gasification of glucose in the presence of 1.0 wt% Raney-nickel at 500^{o}C was examined by Sinag et al. [28] at low heating rates (1and 3^{o}C/min). However, this study was limited to a single reaction temperature and a constant reaction time. In another work, Waldner and Vogel [29] studied the production of methane from woody biomass with Raney-nickel powder. The ratio of the catalyst to reactant was relatively high, i.e. 1:2. The maximum of 33% methane yield was obtained at about 400 8C after 100 min. Furthermore, some researchers investigated the activity of ruthenium as potential catalysts for the gasification of organic compounds in aqueous environments [24]. They found that ruthenium is highly active for reactions involved in super critical water gasification of different biomasses. Comparing with nickel, ruthenium is much more expensive. So, decreasing the amount of ruthenium required for reaction is very important. In our previous work, we compared the performance of ruthenium catalysts prepared with conventional impregnation method [30]. In this study with the aim of increasing performance of the catalysts and increasing the amount of produced hydrogen per gram of Ruthenium, we used microemulsion technique for preparation of the catalysts. Influences of water to surfactant ratio and particle size on the gasification of bagasse will be discussed. To the best of our knowledge, this is the first paper concerning nano-catalytic supercritical water gasification of bagasse.

2. Experimental

2.1. Feed materials

The biomass particles used for the experiments were obtained as shavings, from Haft-Tappe Industries located at Haft-Tappe, Khuzestan, Iran, ground to a particle size ≤ 1 mm in diameter. The elemental composition of the whole biomass sample was analyzed in a CHNS analyzer.

2.2. Catalyst preparation

Conndea Vista Catalox B γ-alumina (200 m^2/g, impurities: Sodium oxide (Na_2O)<0.05 (ppm); Silica (SiO_2)<0.9 (ppm); Sulfate (SO_4)<1.5 (ppm)) was used as support for preparation of the catalysts. Prior to catalyst preparation, the support was calcined at 500°C for 10 h. Two different sets of catalysts were prepared by impregnation and microemultion methods. For all the catalysts the concentration of

ruthenium was adjusted at 5wt.%. The first set of catalysts was prepared by the slurry impregnation method using aqueous solution of ruthenium nitrosil nitrate ($Ru(NO)(NO_3)_3$, Aldrich). After the impregnation step, catalyst was dried at 120°C and calcined at 400°C under Argon flow for 3 h and slowly exposed to atmosphere during the cooling step. The catalysts prepared by this procedure were signified as C_1 (see Table 1).

For the second set of the catalysts, the concentration of ruthenium was also fixed at 5wt.%. The catalysts were prepared by microemulsion technique with aqueous solution of ruthenium nitrosil nitrate ($Ru(NO)(NO_3)_3$, Aldrich). Ruthenium nano particles were synthesized in a reverse microemulsion using a nonionic surfactant Triton X-100 (Chem-Lab), n-hexane (C_6H_{14}, Chem-Lab) as the oil phase and 1-butanol (C_4H_9OH, Merck) as the co-surfactant. The water-to-surfactant molar ratio (W/S) was adjusted at 1.5, 1.0 and 0.5. After vigorous stirring, a microemulsion was obtained (15 min). Hydrazine was added in excess (Hydrazine/Ru = 10) to improve nano particle formation in the core of the micelles by reducing the metal oxides. Then, the appropriate weight of support was added under stirring. During 3 h of stirring, tetrahydrofurane (THF), an emulsion destabilizing agent, was added drop wise (1 ml/min). A fast addition could lead to fast particle agglomeration and uncontrolled particle deposition on the support. The mixture was left to mature and settle slowly overnight and then was decanted. The solid sample was recovered by vacuum filtration using ash less filtration paper (Whatman1) and washed several times with distilled water and ethanol. In order to remove the remaining traces of surfactant and ammonia, the catalysts were dried at 120°C for 2 h and calcined under argon (Ar) flow at 400°C for 3 h and slowly exposed to atmosphere during the cooling step. The catalysts prepared by this procedure were signified as C_2, C_3, and C_4 (see Table 1).

2.3. Catalyst characterization

The metal loadings of the calcined catalysts were performed using Varian VISTA-MPX inductively coupled plasma-optical emission spectrometry (ICP-OES) instrument.

Surface area, pore volume and pores average diameter of the calcined catalysts was measured using an ASAP-2020 V2 Micrometrics system. The samples were degassed at 200°C for 4h under 50 mTorr vacuums and their BET area, pore volume and pore diameter was determined.

The morphology of the calcined catalysts was studied by transmission electron microscopy (TEM). Sample specimens for TEM studies were prepared by ultrasonic dispersion of the catalysts in ethanol, and the suspensions were dropped onto a carbon-coated copper grid. TEM investigations were carried out using a Philips CM20 (100 kV) transmission electron microscope equipped with a NARON energy-dispersive spectrometer with a germanium detector.

The phases and particle sizes of the crystals present in the catalysts were analyzed by XRD using a Philips Analytical X-ray diffractometer (XPert MPD) with monochromatized Cu/Kα radiation, 2θ angles from 10° to 90°. The Debye–Scherer formula was applied to ruthenium oxide peaks at 2θ = 28, in order to calculate the average particle sizes.

The amount of chemisorbed hydrogen on the catalysts was measured using the Micromeritics TPD–TPR 290 system. 0.25 g of the sample was reduced under hydrogen flow at 300°C for 4 h and then cooled to 100°C under hydrogen flow. Then the flow of hydrogen was switched to argon at the same temperature, which lasted about 30 min in order to remove the weakly adsorbed hydrogen. Afterwards, the temperature programmed desorption (TPD) of the samples was obtained by increasing the temperature of the samples, with a ramp rate of 10°C/min, to 300°C under the argon flow. The TPD profile was used to determine the metal dispersion and its surface average crystallite size. After the TPD of hydrogen, the sample was reoxidized at 300°C by pulses of 10% oxygen in helium to determine the extent of reduction.

The calculations are summarized below.

$$\%Dispersion = \frac{H_2\ uptake \times atomic\ weight \times stoichiometry}{\%metal} = \frac{number\ of\ Ru^o\ atoms\ on\ the\ surface \times 100}{total\ number\ of\ Ru^o\ atom} \quad (1)$$

$$Fraction \quad reduced \quad = \frac{O_2 \ uptake \quad (moles \ / \ g.cat.) \times atomic \quad weight}{Percentage \quad metal} \tag{2}$$

$$Diameter(nm) = \frac{6000}{density \times \max imum \ area \times dispersion} \tag{3}$$

2.4. Reaction setup and experimental outline

A batch reactor made of 316 stainless steel tube with total volume of 21 ml has been used in this study. Two series of experiments (catalytic and non-catalytic) are performed. For non-catalytic test, bagasse was mixed with a certain amount of deionized water and injected into the reactor using a syringe. The reactor was plunged in a molten salt bath that contains a mixture of potassium nitrate, sodium nitrate and sodium nitrite. The molten salt bath temperature was controlled using an electrical heater and a PID temperature controller. Temperature and pressure were measured using a K-type thermocouple and a pressure gauge. After a given reaction time, the reactor was taken out of the molten salt bath and plunged in a water bath for rapid cooling to room temperature. For catalytic tests, certain amount of catalyst is charged to the reactor. The catalyst was then reduced in flowing hydrogen for 4 h (50 ml STP/min H_2) before addition of bagasse and deionized water. All experiments were performed 3 times under the same experimental conditions and the data reported here are the averages of repetitive runs. In this study, the influence of catalyst on the gasification of bagasse was investigated. At the end of each experiment, reactor free volume, final pressure and temperature were used to calculate the gas yield. The amounts of each product gases were measured and analyzed using gas chromatographs (Varian 3400 and Teyfgostar-Compact). For each experiment, the carbon gasification ratio (CGR) which is the ratio of the amount of carbon in the gaseous products to the amount of carbon in the bagasse and hydrogen gasification ratio (HGR) which is the ratio of the amount of hydrogen in the gas phase to the amount of hydrogen in the bagasse were measured after each experiment. Mathematically, CGR and HGR are defined as:

$$CGR = \{Y_{CO}+Y_{CH4}+Y_{CO2} + 2Y_{C2H4}+ 2Y_{C2H6}\}/\{\text{mmol Carbon /g bagasse}\} \tag{4}$$

$$HGR = \{Y_{H2}+2Y_{CH4}+2Y_{C2H4}+3Y_{C2H6})/\{\text{ mmol } H_2 \text{ /g bagasse}\} \tag{5}$$

3.Results and Discussion

3.1. Catalysts characterization

The elemental compositions of the calcined catalysts measured by ICP are given in Table 1. This table shows that the metal contents of the catalysts were fairly similar and close to the targeted metal contents.
Results of surface area measurements for the calcined catalysts are given in the Table 1. These results show that the BET surface areas of the C_2-C_4 catalysts (prepared by microemulsion) are 236.2-252.7 m^2/g. However, the BET surface area for the C_1 catalyst (prepared by impregnation) is somewhat lower (202.3-m^2/g), which indicates some more pore blockage by metal oxide clusters in the catalyst prepared by impregnation method than the catalysts prepared by microemulsion method. This table also shows that the BET surface area of the catalysts prepared by micro emulsion increases by decreasing the W/S ratio indicating smaller ruthenium particles and lesser pore blockage by ruthenium oxide clusters in the case of the catalysts prepared with lower W/S ratios.
The TEM image of C_1 catalyst prepared by impregnation method is shown in figure 1a. This figure shows that the particles are distributed on surface of the support pores. The sizes of particles are within the range of 6–15nm. The TEM images of C_2-C_4 catalysts prepared by the microemulsion method are shown in figures 1b-1d. As shown, very small particles are dispersed on surface of the support pores. The sizes of particles are within the range of 5–9, 4-8 and 2-6 nm for the C_2, C_3 and C_4 catalysts, respectively. Based on the TEM pictures, the average particle size for the C_1, C_2, C_3 and C_4 catalysts are 11, 6.4, 4.6 and 3.1 nm respectively. Of particular importance, the particle size distribution is too narrow in the case of the catalysts prepared by microemulsion method.

Table 1: Chemical composition, preparation details and textural properties of the calcined catalysts

Sample	Preparation route	W/S Ratio	Targeted composition (wt.%)	Measured composition (wt.%)	BET surface area (m^2/g)	Total pore volume (ml/g)	Average pore diameter (Å)
Support	-	-	-	-	275.6	0.758	11
C_1	Impregnation	-	5	4.92	202.3	0.573	10.16
C_2	Microemulsion	1.5	5	4.86	236.7	0.656	10.49
C_3	Microemulsion	1	5	4.86	243.1	0.660	10.54
C_4	Microemulsion	0.5	5	4.89	252.7	0.673	10.66

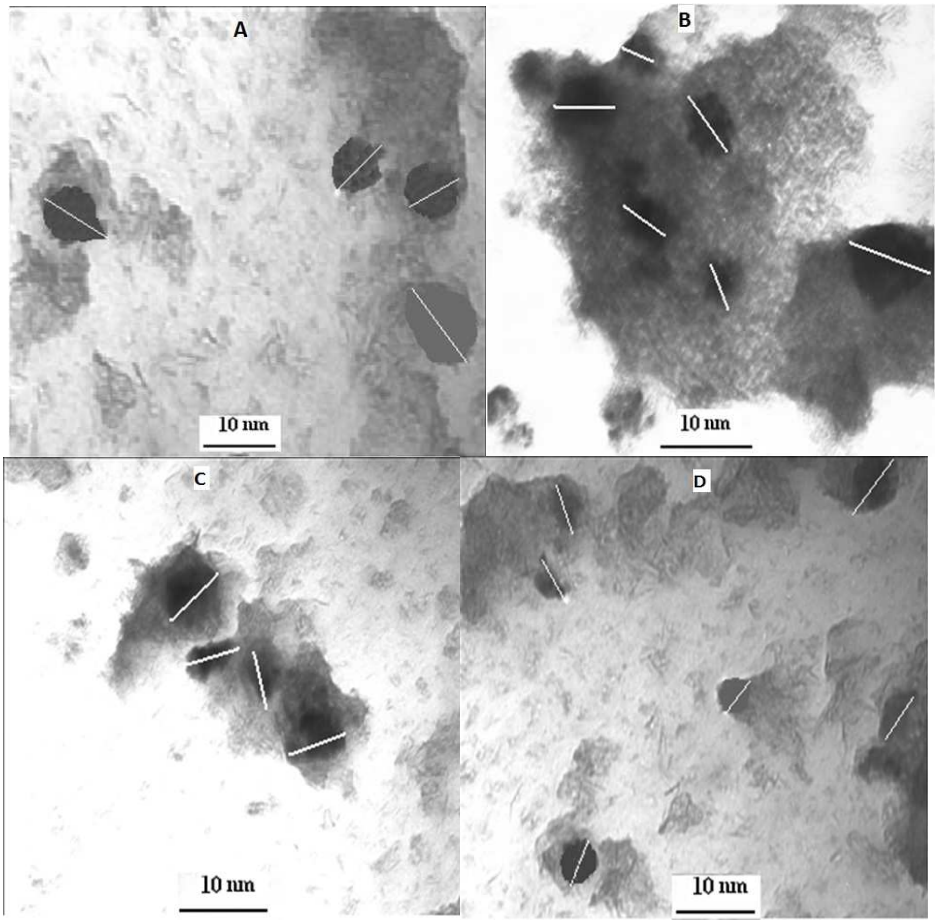

Figure 1a-d: TEM images of C1 , C2 , C3 and C4 catalysts

To determine the crystalline phases, X-ray diffraction experiments (XRD) of the calcined catalysts were performed. XRD patterns of the catalysts are shown in Figure 2. In the XRD spectra of all the catalysts, the peaks at 2θ values of 36.3°, 38.7°, 45.6° and 66.6° correspond to the support, while the other peaks in the

spectra of the catalysts are related to different crystal planes of ruthenium oxide (peaks at 2θ values of 28°, 35° and 54.3°). The peak at 28° is the most intense peak of ruthenium oxide in XRD spectrum of all the catalysts. Table 2 shows the average ruthenium oxide cluster size for the catalysts calculated from XRD spectrum and Scherer equation. According to table 2, the average ruthenium oxide cluster size for the catalysts synthesized by microemulsion are significantly lower compared to the catalyst prepared by impregnation method, indicating better dispersion of metal clusters. Also, in the case of the catalysts prepared by microemulsion, the average ruthenium oxide cluster size was decreased from 5.7 to 3.8 nm by decreasing the W/S ratio from 1.5 to 0.5. The average particle sizes of ruthenium oxide are linearly correlated with the water-to-surfactant ratio used during the microemulsion catalyst preparation route. In fact, nanoparticles are formed in the internal structure of the microemulsion, which is determined by the ratio of water-to surfactant. At high oil concentration, the bicontinuous phase is transformed into a structure of small water droplets within a continuous oil phase (reverse micelles) when surfactant is added. Thus, the results show that the size of different droplets determines the metal's particle size, depending on the amount of surfactant [6-8].

The results of chemisorption and re-oxidation tests are given in Table 2. This table shows that, using microemulsion considerably increases the percentage dispersion. For the catalysts prepared with microemulsion method, percentage dispersion increases with decreasing W/S ratio. Maximum dispersion is achieved at the minimum W/S ratio of 0.5. The average particles diameter decreased (from 6.5 to 3.9 nm), which are in agreement with the results of XRD and TEM tests. Also, the percentage reduction of the catalysts shows a considerable increase (about 29% enhancement). Higher dispersions, smaller metal cluster sizes and higher degrees of reduction in the case of the catalysts prepared by microemulsion will increase the number of sites available for reaction.

Table 2: XRD and H2 chemisorption results for the calcined catalysts

Catalyst	%Reduction	%Dispersion	dP (nm)	dp(nm) calculated by Debye–Scherer formula
C1	69.5	53.8	6.5	8.6
C2	85.7	72.8	4.8	5.7
C3	87.3	83.2	4.2	4.9
C4	89.6	89.6	3.9	3.8

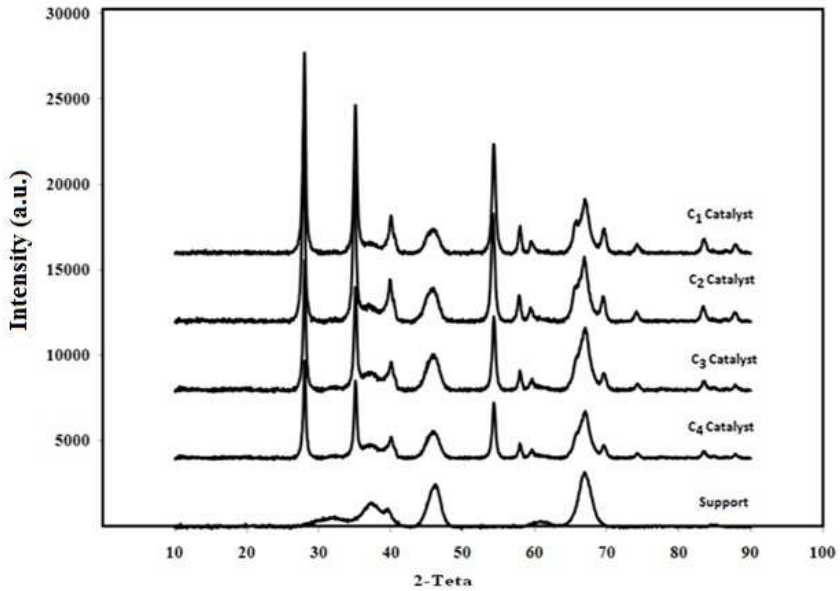

Figure 2: X-ray diffraction patterns of the calcined catalysts and support

Table 3: The non-catalytic gasification yields (mmolof gas /g of bagasse) for the whole gaseous products and H2, CO, CO2, CH4 and heavier hydrocarbons (T=400oC, Reaction time= 5 min, bagasse loading: 0.05 g, water loading: 4 g).

Total Gas	19.2
H2	7.13
CO2	5.96
CO	6.04
CH4	0.035
Heavier Hydrocarbon	0.029

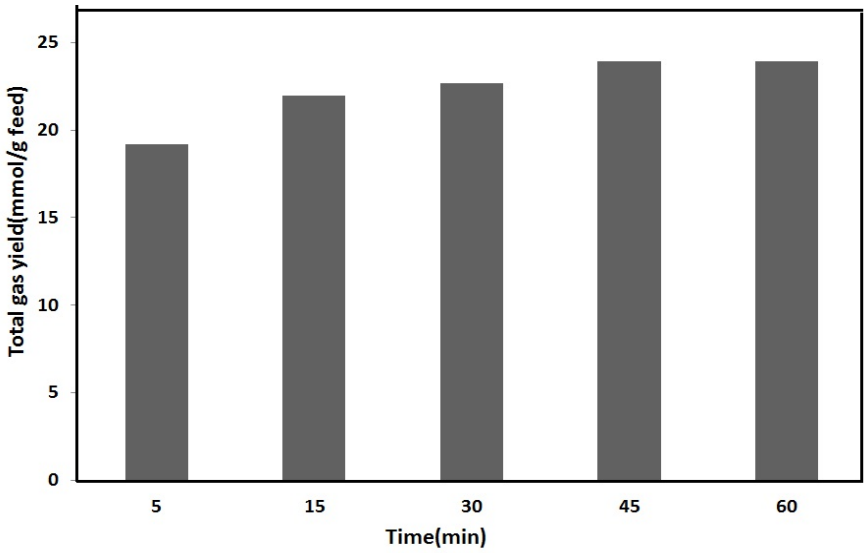

Figure 3: The non-catalytic total gasification products yield versus reaction time (T:4000C, bagasse loading: 0.05 g, water loading: 4 g).

3.2. CHNS analyses of bagasse

The CHNS analyses of the biomasses were N = 0.69%, C = 58.10%, H = 6.45%, S= 0.19% and O = 34.57%. The C and H content in the sample was 64.55%. The balance was mostly oxygen.

3.3. Reaction

In order to determine the time required for gasification of bagasse, the effects of reaction time on conversion and product gas composition have been studied at the temperature of 400°C, reaction time of 15 min, feed content of 0.05g and water loading of 4 g. Afterwards, the effects of catalyst type and on the gasification yield and products selectivity have been studied at the determined reaction conditions.

Reaction time is varied by increasing the duration of SCW gasification process from 5 to 60 min after the temperature of the reactor reaches its maximum. Table 3 presents the gasification yields (mmol of gas/g of bagasse) for the whole gaseous products and H_2, CO, CO_2, CH_4 and heavier hydrocarbons at reaction time of 5 min for bagasse loading of 0.05 g and water loading of 4 g.

It is referred by different authors that, the biomass gasification in SCW is a complex process, but the overall chemical conversion can be represented by the simplified net reaction:

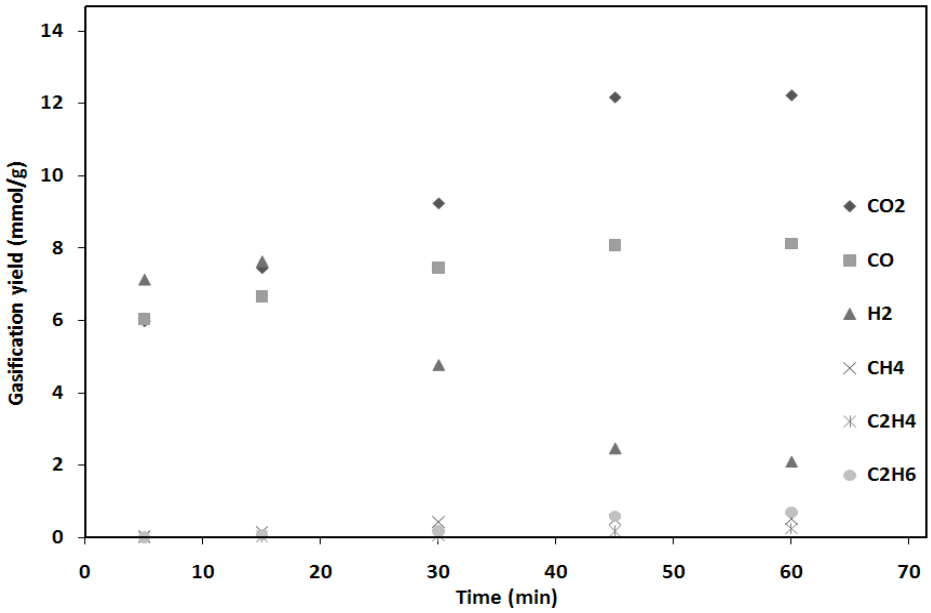

Figure 4: The non-catalytic bagasse product gasification yields versus reaction time (T:400°C, bagasse loading: 0.05 g, water loading: 4 g).

$$CH_xO_y + (2\text{-}y)\ H_2O \rightarrow CO_2 + (2\text{-}\ y+x/_2)\ H_2 \quad (6)$$

Where x and y are the elemental molar ratios of H/C and O/C in biomass, respectively. The reaction product is syngas whose quality depends on x and y. The reaction (6) is an endothermic reaction. It is known from the reaction (6) that water is not only the solvent but also a reactant and the hydrogen in the water is released by the gasification reaction. Equation (6) summarizes the overall reaction, but a group of competing intermediate reactions, which are essential for the successful gasification; need to be considered as follows:

Steam reforming: $CH_xO_y + (1\text{-}y)\ H_2O \rightarrow CO + (1\text{-}\ y+x/_2)\ H_2$ (7)

Water-gas shift: $CO + H_2O \leftrightarrow CO_2 + H_2$ (8)

Methanation: $CO + 3H_2 \leftrightarrow CH_4 + H_2O$ (9)

The results on table 3 shows that, the final product gas composition of the bagasse SCW gasification process is the result of combination of the above mentioned series of complex and competing reactions.
Figures 3 and 4 depict the effect of reaction time on the SCW gasification products. It is seen that, the amount of generated gas increases as reaction time increases from 5 to 45 min but no significant change in the conversion occurred by extending the reaction time to 60 min. As shown in figure 4, the hydrogen yield increases by increasing the reaction time, reaches a maximum at reaction time of 15 min and then starts to decrease sharply. Also, extending the reaction time increases the methane yield from 0.035 to 0.52 mmol/g of bagasse. As the reaction time increased from 5 to 45 min, the methane yield increased significantly, while the total gasification yield increased by a factor of 1.25. Although, beyond 45 min reaction time, the total yield of the product gas is not changed, the composition continued to change slightly. The decrease in H_2 yield and increase in the methane yield can be attributed to methanation process (equation 9). According to the reaction 9, consuming three mole H_2 generates one mole CH_4 and consumes one mole CO. Therefore downward trend of H_2 yield should be sharper than rising trend of CH_4 and CO yields. When the objective of biomass gasification in SCW is hydrogen production, the reaction (9) must be restrained and CO reacting with water to form CO_2 and H_2 is desired (reaction 8) must be affectionate.

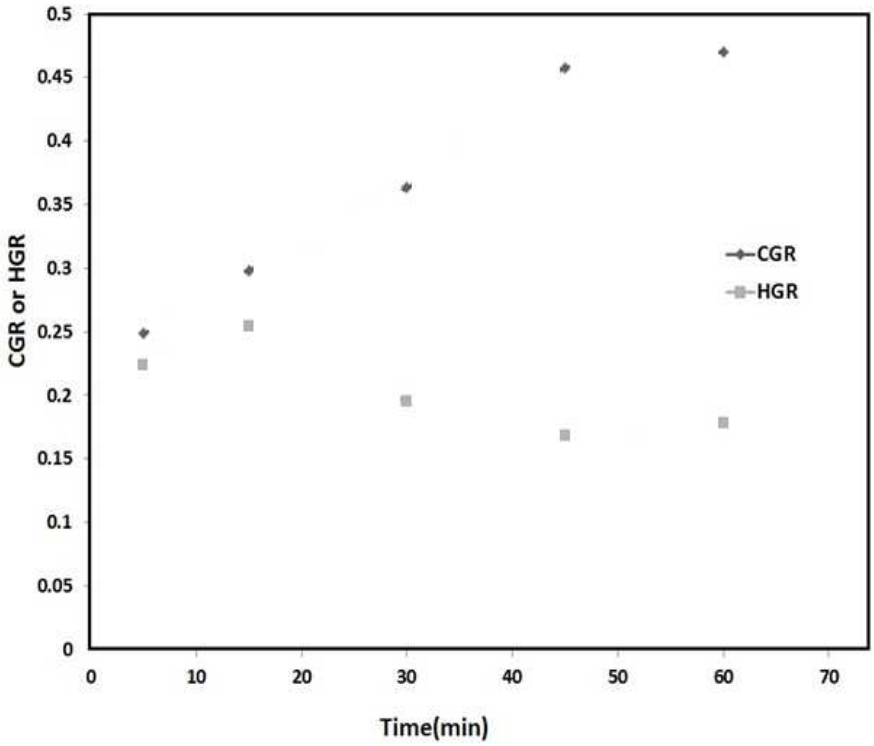

Figure 5: The non-catalytic CGR and HGR versus reaction time (T:4000C, bagasse loading: 0.05 g, water loading: 4 g).

Figure 4 also shows that the yield of CO_2 increases as reaction time increases from 3 to 45 min but no significant change in the CO_2 yield occurred by extending the reaction time to 60 min. This figure also shows that the yield CO increases with time slightly which is due to increase in bagasse conversion with time.

Figure 5 show the CGR and HGR values calculated using the gasification. As shown, the HGR increased by increasing the reaction time, reached a maximum of 0.254 at reaction time of 15 min and then sharply started to decrease. Since the aim of this work is to maximize the hydrogen yield, reaction time of 15 min was selected as the optimum reaction time. While by increasing the reaction time from 5 to 60 min, the CGR just about doubled.

Figure 6 shows the gas yields (mmol of gas/g of bagasse) for the whole gaseous products obtained from the gasification of bagasse at 400^{o}C in the presence of catalysts. From this figure and figure 3 it becomes apparent that the addition of catalyst increased the gas production by a factor of 1.6-2.3, depending on the catalyst type. This figure reveals that the performances of the catalysts prepared with microemulsion method are significantly higher than that of the catalyst prepared by impregnation. Catalyst prepared with minimum water to surfactant ratio of 0.5 shows the highest activity. It should be noted that the weight percent of active metal in all catalysts are the same. Figure 6 also shows the number of active ruthenium sites for the catalysts prepared by impregnation and microemulsion methods. Number of active ruthenium sites was defined as:

$$\text{Number of active Ru sites} = \text{wt. of Ru} \times \text{Frac. Red.} \times \text{Disp.} \times \text{NA} \times \text{MW} \qquad (10)$$

Where NA is Avogadro's number and MW is molecular weight of ruthenium. This figure reveals that using microemulsion especially in low water to surfactant ratios increases the number of active metal sites. The trend for the total gas yields is similar to that for the number of active metal sites. The gas yields increases in accordance with the number of active ruthenium sites. The maximum gas yield is achieved with the minimum water to surfactant ratio and highest number of active ruthenium sites.

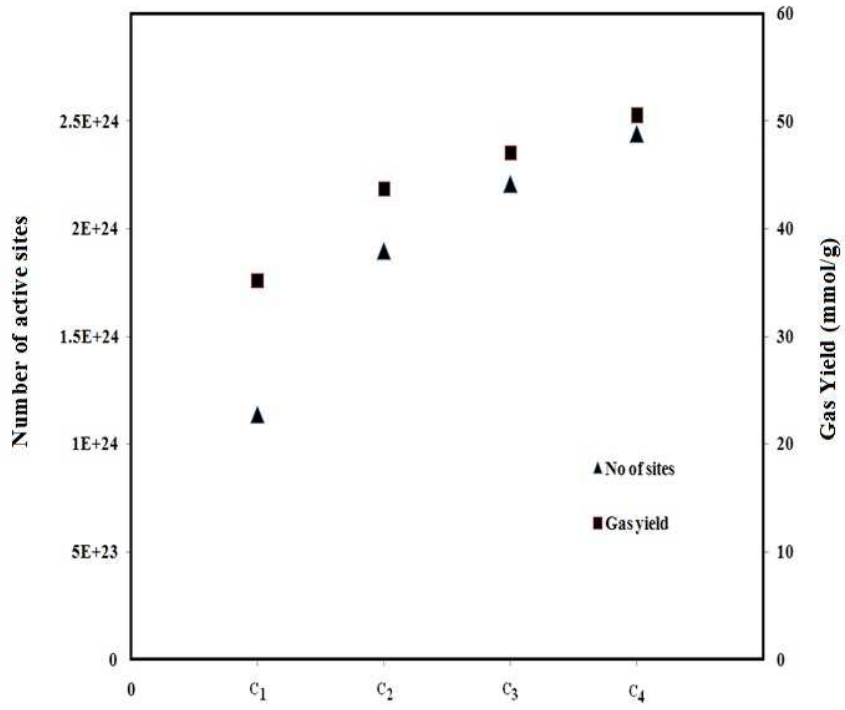

Figure 6: Variation of total gas yields (mmol of gas/g of bagasse) and number of active sites for different catalysts (T:4000C, bagasse loading: 0.05 g, water loading: 4 g).

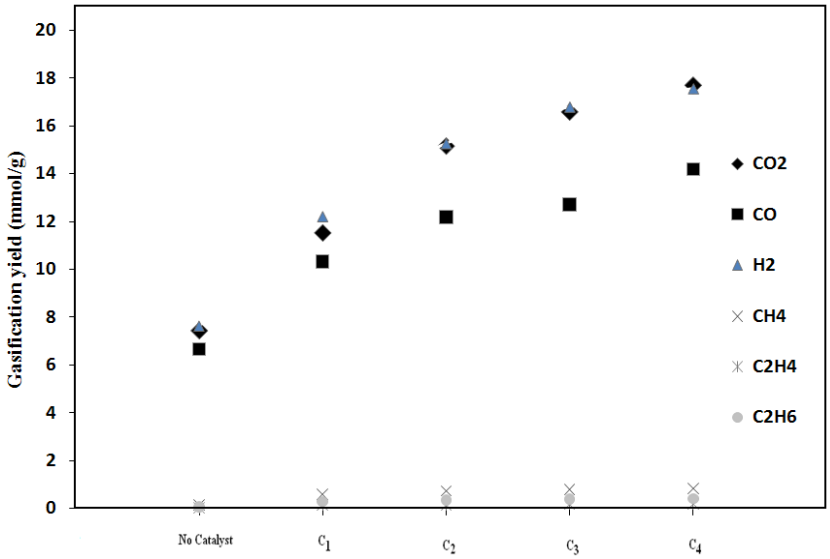

Figure 7: The product gasification yields versus catalyst type (T:4000C, bagasse loading: 0.05 g, water loading: 4 g).

This figure reveals that the gasification activity of the catalysts is strongly proportional to the number of surface reduced ruthenium sites. Therefore, the maximum concentration of surface Ru° sites and gasification activity is achieved for the C_4 catalyst presenting the lowest average ruthenium particle sizes, best dispersion and highest reducibility. In addition, improvement of the uniformity of the catalyst particles by decreasing the water to surfactant ratio, leads to a better stability of the products and the gasification activity.

Table 4: The catalysts specific activity (mmol of hydrogen /g of Ru) (T=400°C, Reaction time= 5 min, bagasse loading: 0.05 g, water loading: 4 g).

Catalyst	Catalysts specific activity (mmol/g)
C_1	4964
C_2	6205
C_3	6826
C_4	7136

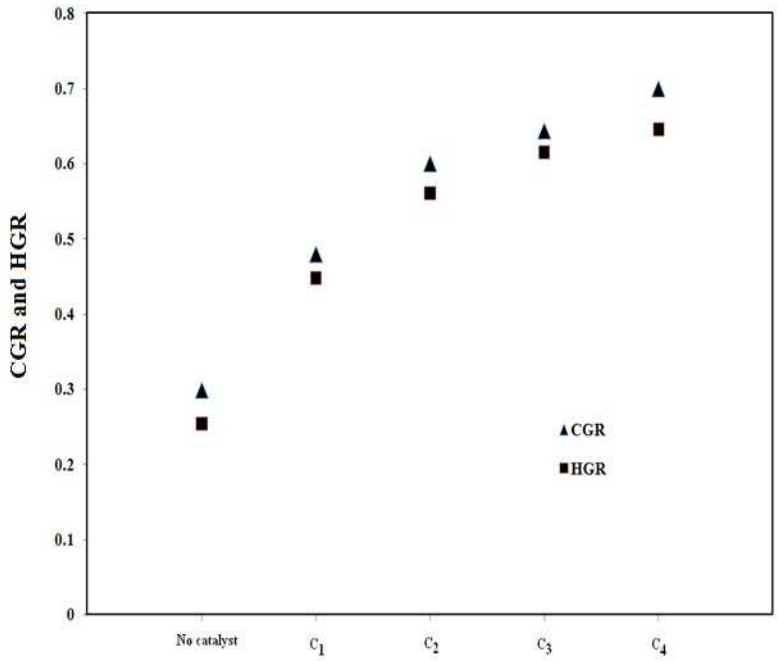

Figure 8: Variation of CGR and HGR for different catalysts (T:4000C, bagasse loading: 0.05 g, water loading: 4 g).

Figure 7 shows the gas yields of hydrogen, carbon monoxide, carbon dioxide, methane and light gaseous hydrocarbons obtained from the gasification of bagasse at 400°C in the presence of catalyst. As shown addition of C_1 catalyst (prepared with impregnation) increased the methane production by a factor of 3.9 while the C_2, C_3 and C_4 catalysts (prepared by microemulsion) with the same Ru loading) increased the methane production by a factor 4.89, 5.3 and 5.7, respectively. The same trend can be seen for light gaseous hydrocarbons. At the same time, C_1 catalyst increased the hydrogen production by a factor of 1.60 while the C_2, C_3 and C_4 catalysts increased the hydrogen production by a factor 2.0, 2.2 and 2.3, respectively. As shown the increase in the methane formation is higher than that of the hydrogen. It is demonstrated that ruthenium is highly active for the hydrogenation of CO and CO_2 and the catalyst with higher Ru dispersion is more active for cleaving C-O bonds compared to the catalyst prepared with impregnation method. Higher dispersion of ruthenium in the case of the catalysts prepared with microemulsion method enhances the hydrogenation of CO and CO_2 which in turn leads to low increase in the hydrogen production as compared to methane production.

The CGR and HGR values were calculated from the gasification data and shown in figure 8. The results show that maximum hydrogen gasification ratio of 0.65 is achieved for catalyst prepared with microemulsion and minimum water to surfactant ratio of 0.5. This catalyst also increased the CGR by a factor of 2.34.

The catalyst specific activity is defined as the amount of hydrogen produced (mmol) to the amount of Ru (gram) in the catalysts. Table 4 shows the specific activity of the catalysts. As discussed earlier, the

ruthenium loading for all catalysts are the same. Table 4 shows that using microemulsion technique for preparation of the catalysts increases the catalyst specific activity (m mol of H_2/ gram of Ru) by a factor of 1.7. Therefore, it can be concluded that using this technique for preparation of catalysts will enhance the economic aspects of the bagasse super critical water gasification technology.

4. Conclusions

The supercritical water gasification of bagasse was studied using a batch micro reactor in the presence of the Ru/Al_2O_3 nano catalysts. The catalysts are prepared using impregnation and microemulsion techniques. It was observed that using microemulsion technique increases the total gas yield significantly. Maximum hydrogen yield of 17.6 (mmol of H_2/ gram of bagasse) is observed for the catalyst prepared with water to surfactant ratio of 0.5. It was observed that using micro emulsion technique increases the catalyst specific activity by a factor of 1.7 that considerably will enhance the economic aspects of the bagasse super critical water gasification technology.

5. References

[1] Tavasoli A, Ahangari MG, Soni C, Dalai A.K., Fuel Processing Technology. 90 (2009) 472-82.
[2] Williams PT, Onwudili J., Industrial and Engineering Chemistry Research. 44 (2005) 8739-49.
[3] Voll FAP, Rossi CCRS, Silva C, Guirardello R, Souza ROMA, Cabral V.F. , International Journal of Hydrogen Energy. 34 (2009) 9737-44.
[4] Hendry D, Venkitasamy C, Wilkinson N, Jacoby W., 102 (2011) 3480-7.
[5] Hao X, Guo L, Zhang X, Guan Y. , Chemical Engineering Journal. 110 (2005) 57-65.
[6] Azadi P, Khan S, Strobel F, Azadi F, Farnood R. , Applied Catalysis B: Environmental. 117 (2012) 330-8.
[7] Resende FLP, Savage PE. , 49 (2010) 2694-700.
[8] Guo LJ, Lu YJ, Zhang XM, Ji CM, Guan Y, Pei AX. , Catalysis Today. 129 (2007) 275-86.
[9] Yanik J, Ebale S, Kruse A, Saglam M, Yüksel M. , Fuel. 86 (2007) 2410-5.
[10] Wang Y, Kinoshita CM. , Solar Energy. 49 (1992) 153-8.
[11] Turn S, Kinoshita C, Zhang Z, Ishimura D, Zhou J., International Journal of Hydrogen Energy. 23 (1998) 641-8.
[12] Ferdous D, Dalai AK, Bej SK, Thring RW, Bakhshi NN., Fuel Processing Technology. 70n (2001) 9-26.
[13] Hanaoka T, Inoue S, Uno S, Ogi T, Minowa T., 28 (2005) 69-76.
[14] Soni CG, Dalai AK, Pugsley T, Fonstad T., Asia-Pacific Journal of Chemical Engineering. 6 (2011) 71-7.
[15] Ferdous D, Dalai AK, Bej SK, Thring RW., Canadian Journal of Chemical Engineering. 79 (2001) 913-22.
[16] Dalai AK, Batta N, Eswaramoorthi I, Schoenau GJ., Waste Management. 29 (2009) 252-8.
[17] Lv PM, Xiong ZH, Chang J, Wu CZ, Chen Y, Zhu JX., Bioresource Technology. 95 (2004) 95-101.
[18] Franco C, Pinto F, Gulyurtlu I, Cabrita I. , Fuel. 82 (2003) 835-42.
[19] Wei L, Xu S, Zhang L, Liu C, Zhu H, Liu S. , International Journal of Hydrogen Energy. 32 (2007) 24-31.
[20] Xiao R, Jin B, Zhou H, Zhong Z, Zhang M. , Energy Conversion and Management. 48 (2007) 778-86.
[21] DeGroot WF, Richards GN. , Carbon. 27 (1989) 247-52.
[22] Devi L, Ptasinski KJ, Janssen FJJG, Van Paasen SVB, Bergman PCA, Kiel JHA. , Renewable Energy. 30 (2005) 565-87.
[23] Bridgwater AV. , Fuel. 74 (1995) 631-53.
[24] Azadi P, Khodadadi AA, Mortazavi Y, Farnood R., Fuel Processing Technology. 90 (2009) 145-51.
[25] Lu YJ, Guo LJ, Ji CM, Zhang XM, Hao XH, Yan QH. , International Journal of Hydrogen Energy. 31 (2006) 822-31.
[26] Ding ZY, Frisch MA, Li L, Gloyna EF., Industrial and Engineering Chemistry Research. 35 (1996) 3257-79.
[27] Al-Duri B, Pinto L, Ashraf-Ball NH, Santos RCD. , Journal of Materials Science. 43 (2008) 1421-8.
[28] Sinag A, Kruse A, Rathert J., Ind. Eng. Chem. Res. 43 (2004) 502-509.
[29] Waldner M, Vogel F, Ind. ENG. Chem. Res. , 44 (2005) 4543-4551.
[30] Rashidi M., Tavasoli A. , Petroleum & Coal, 56(3), (2014) 311-319.